Supporting Information

Transforming $Mo_{0.5}W_{0.5}O_3$ to MoS_2: Leveraging Selective Sulfurization for Enhanced Electrocatalysis

Naveen Goyal [a], Gokul Raj [a], Karuna Kar Nanda [a], and N. Ravishankar [a,*]

[a] Materials Research Centre, Indian Institute of Science, Bangalore-560012, India

[*]Corresponding author: nravi@iisc.ac.in

Table S1. Lattice parameters of hydrated WO_3, MoO_3 and $W_{0.5}Mo_{0.5}O_3$.

Compound	Lattice Parameters		
	a (Å)	b (Å)	c (Å)
WO_3 0.33H_20	7.35	12.51	7.70
MoO_3 0.33H_20	7.33	12.67	7.69
$W_{0.5}Mo_{0.5}O_3$ 0.33H_20	7.34	12.59	7.695

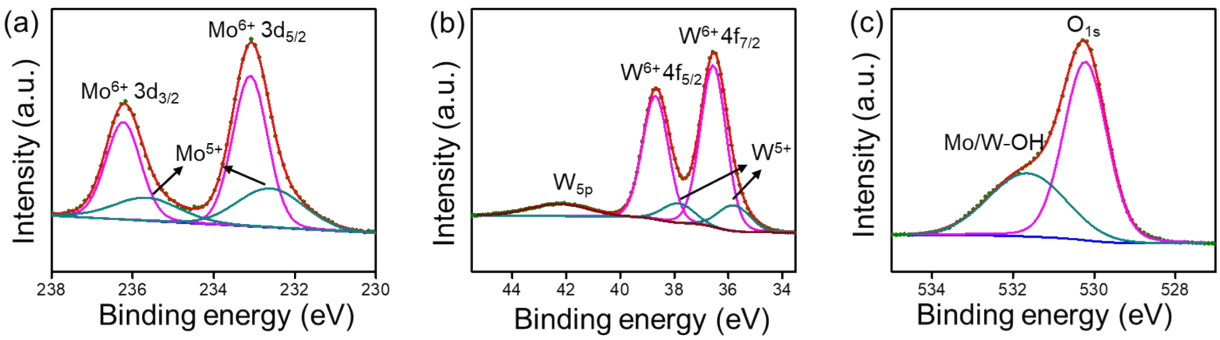

Figure S1. XPS spectra of **(a)** Mo 3d, **(b)** W 4f, and **(c)** O 1s of template $W_{0.5}Mo_{0.5}O_3$ 0.33H_20.

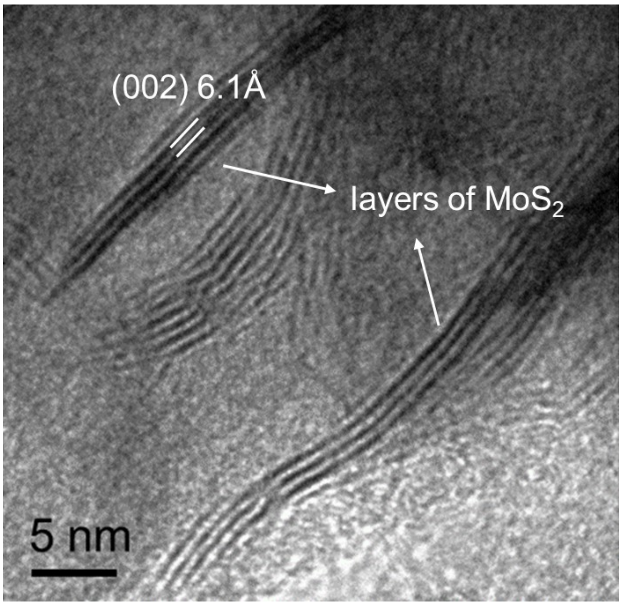

Figure S2 High resolution TEM micrograph showing layers of MoS_2 in final selectively sulfurized product.

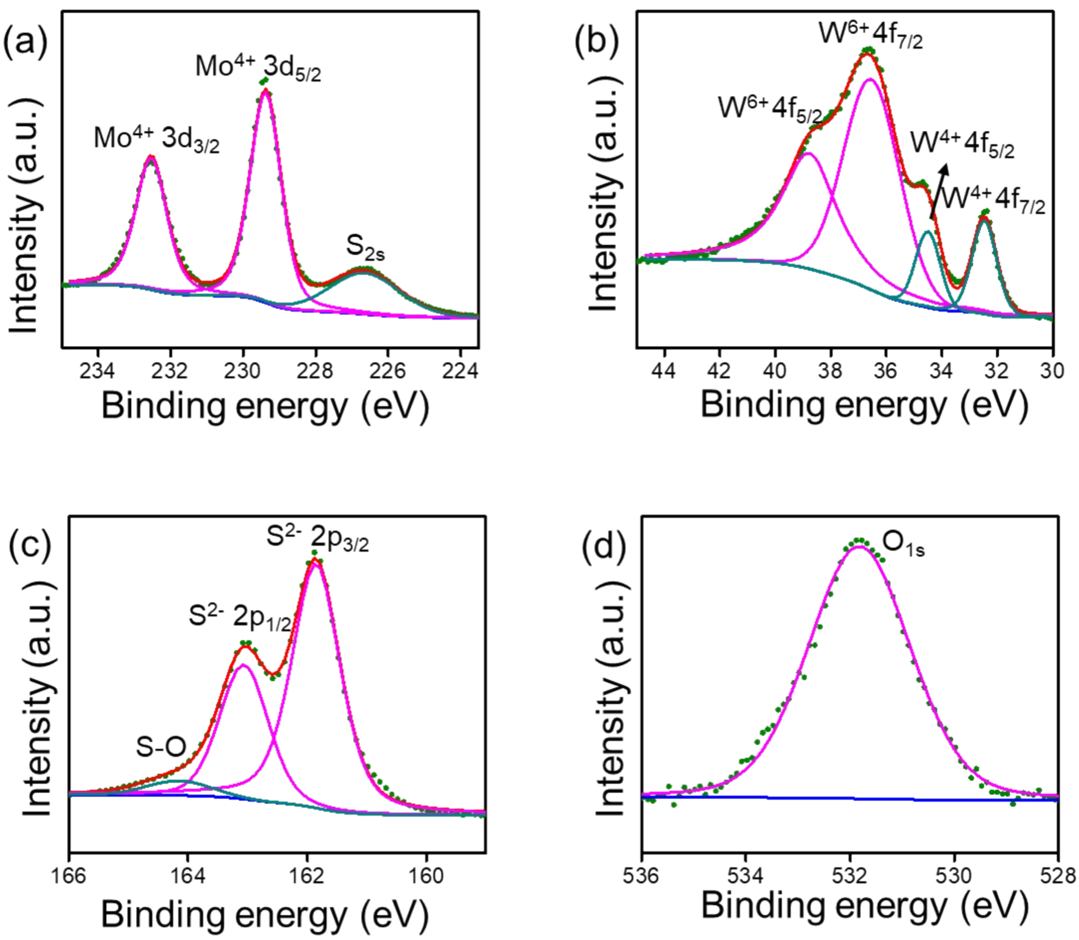

Figure S3. High resolution XPS spectra of **(a)** Mo 3d, **(b)** W 4f, **(c)** S 2p, and **(d)** O 1s of final selective sulfurized product.

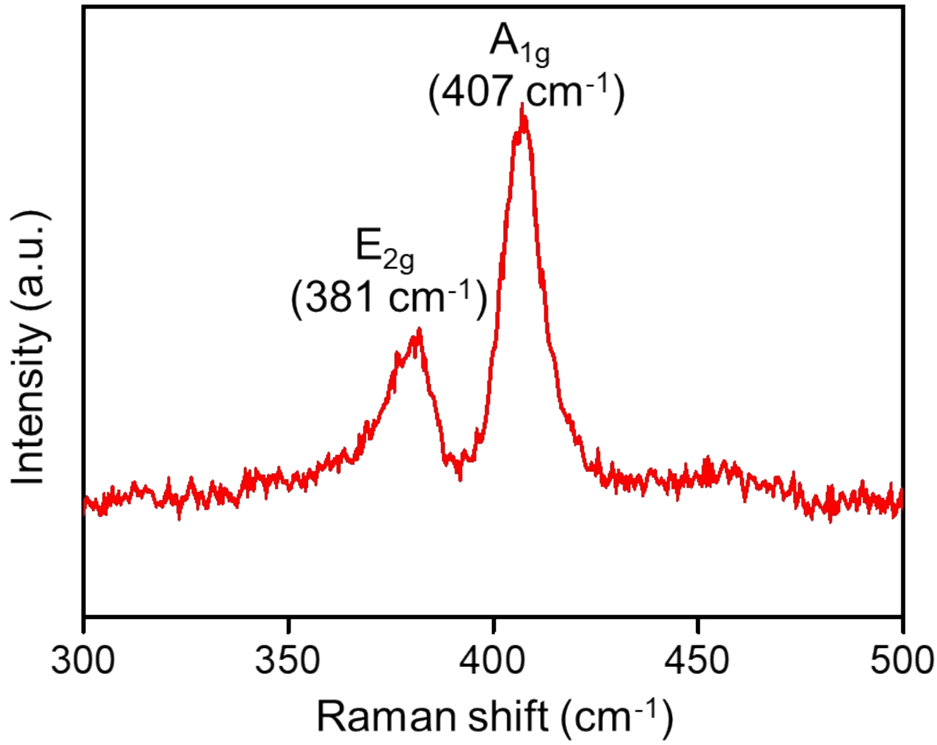

Figure S4: Raman spectra of selective sulfurized product depicting formation of only MoS_2.

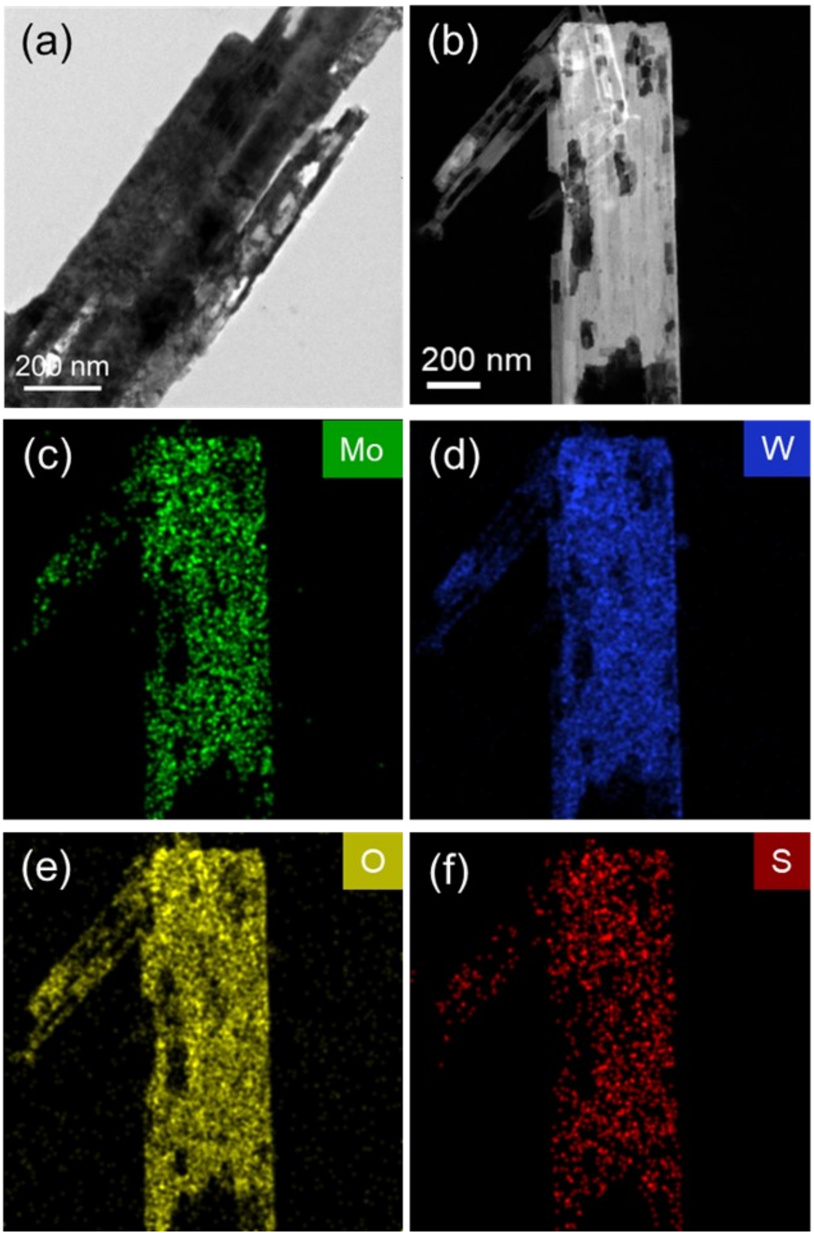

Figure S5. Time dependent experiment; **(a)** BF-TEM micrograph of 3 h sulfurized product, **(b)** corresponding HAADF-STEM micrograph and EDS maps showing elemental distribution of Mo **(c)**, W **(d)**, O **(e)**, and S **(f)**, respectively.

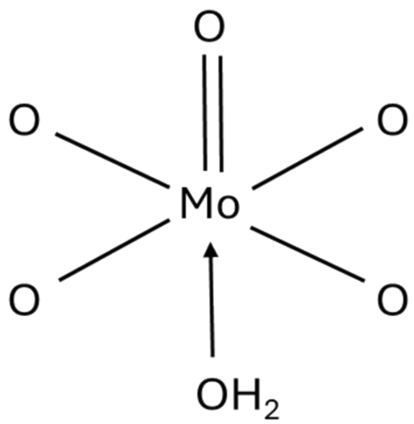

Figure S6. Structural arrangement of Mo in octahedral environment of O and H_2O in pristine $W_{0.5}Mo_{0.5}O_3$ $0.33H_20$.

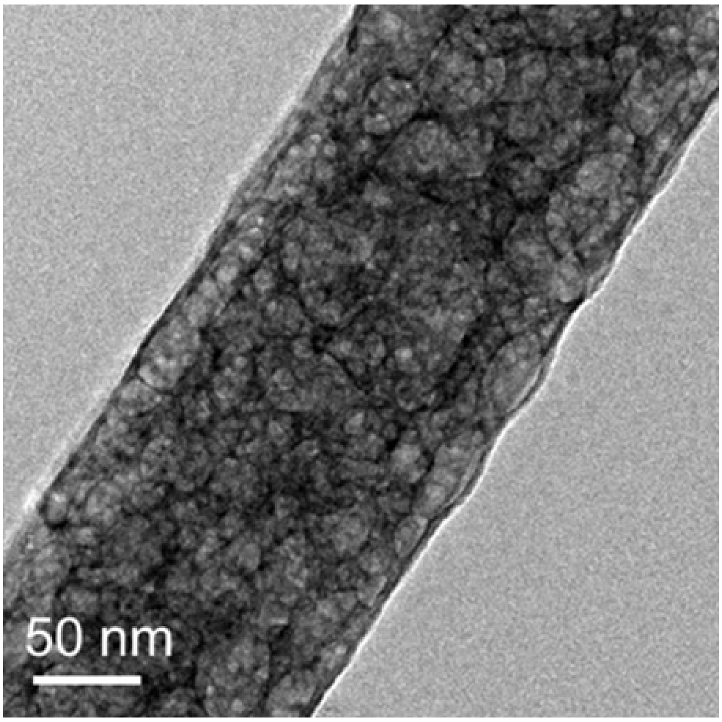

Figure S7. BF-TEM micrograph of 6 h sulfurized product showing formation of MoS_2-WO_3 heterostructure.

Table S2. Calculated binding energies and % abundance of various oxidation states of Mo in XPS analysis of 6 h sulfurized product.

Mo	Oxidation state	Binding energy (eV)	Peak area	Total area of each oxidation state	% abundance of each oxidation state
$3d_{3/2}$	+6	236.0	26489	66624	51.3
$3d_{5/2}$		232.9	40135		
$3d_{3/2}$	+4	234.6	25170	63306	48.7
$3d_{5/2}$		231.5	38136		

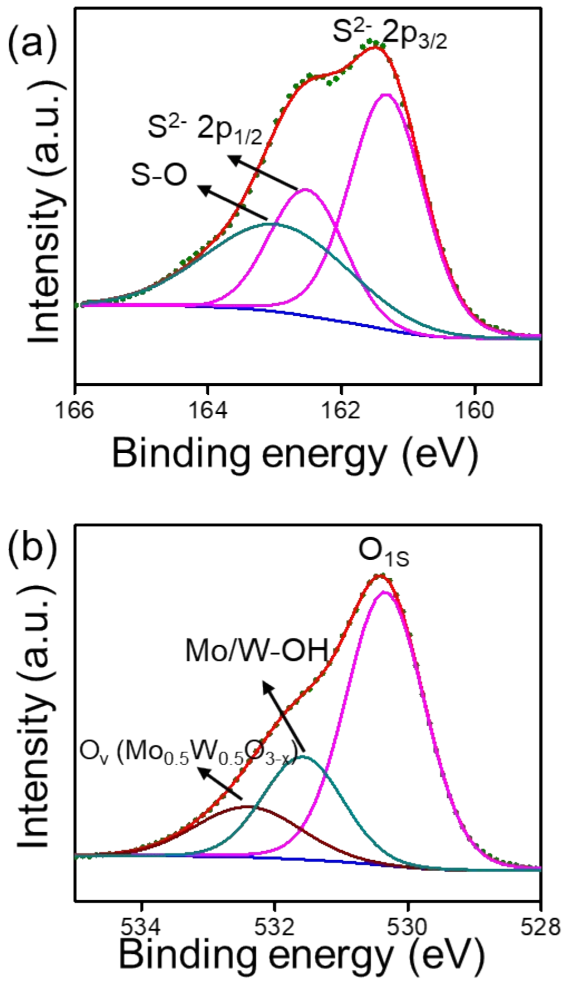

Figure S8. High resolution XPS spectra of **(a)** S 2p, and **(b)** O 1s of 6 h sulfurized product.

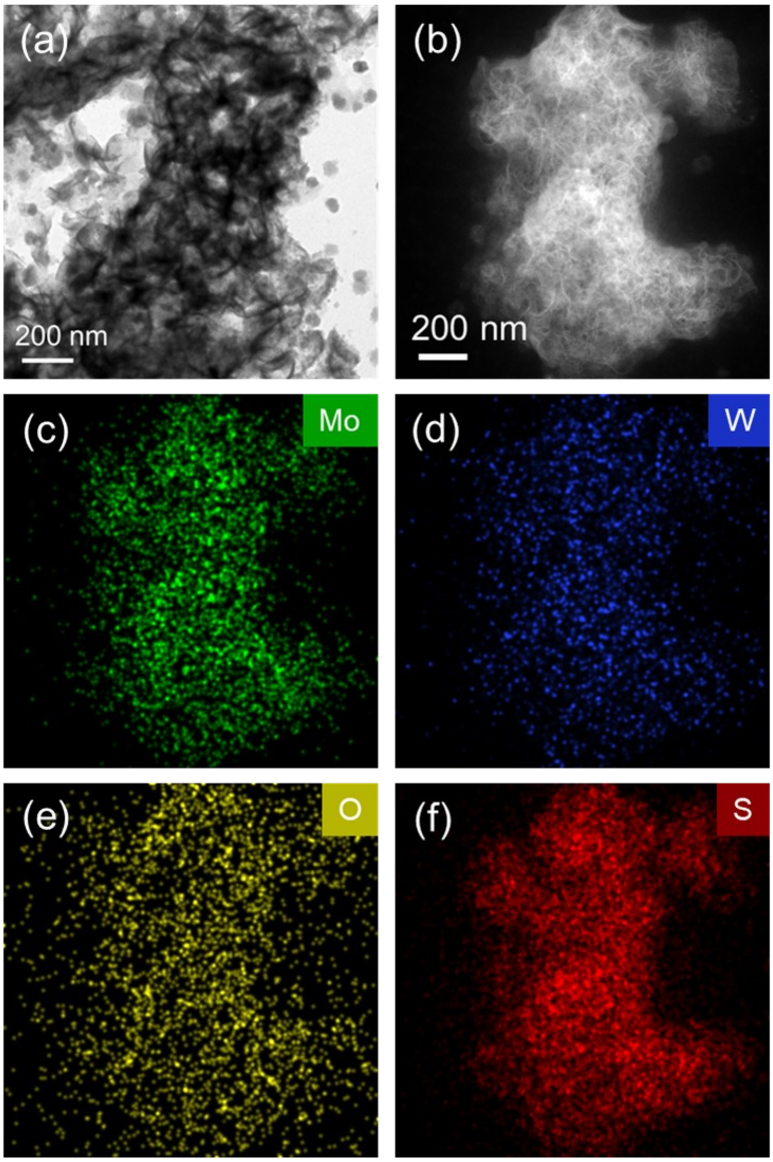

Figure S9. Time dependent experiment; **(a)** BF-TEM micrograph of 12 h sulfurized product, **(b)** corresponding HAADF-STEM micrograph and EDS maps showing elemental distribution of Mo **(c)**, W **(d)**, O **(e)**, and S **(f)**, respectively.

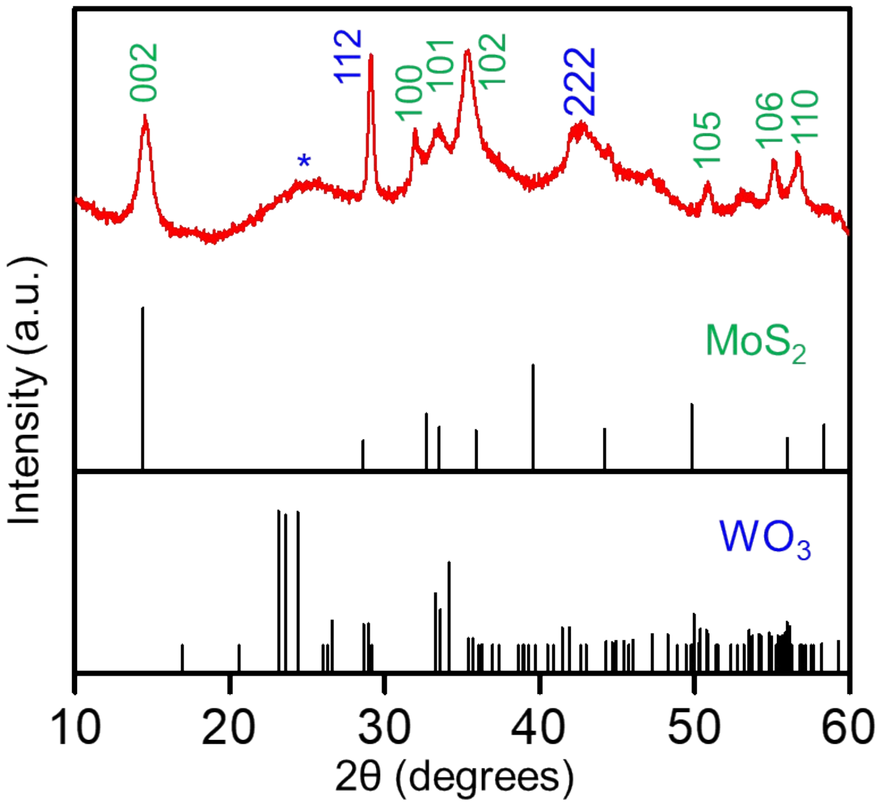

Figure S10. PXRD pattern of 12 h sulfurized product depicting co-existence of MoS_2 (major) and WO_3 (minor).

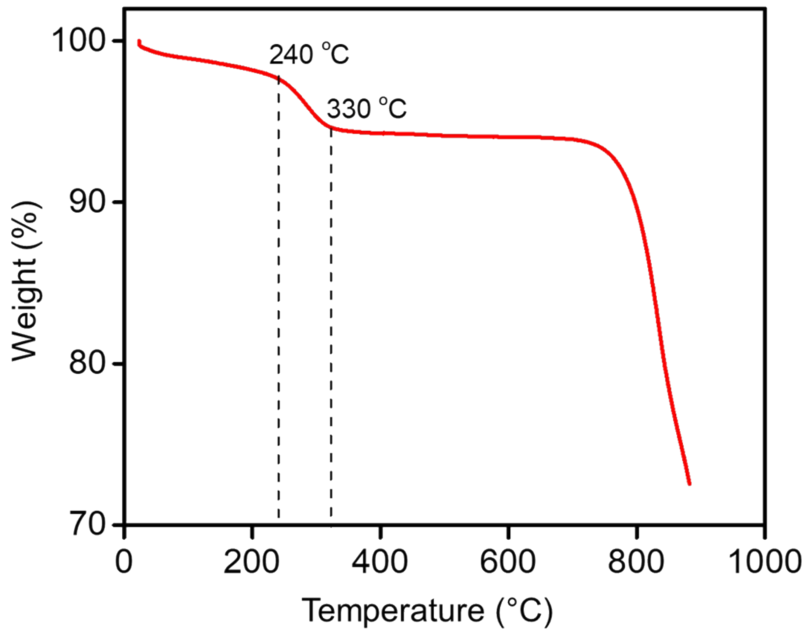

Figure S11: TGA plot of template $W_{0.5}Mo_{0.5}O_3$ 0.33H_20.

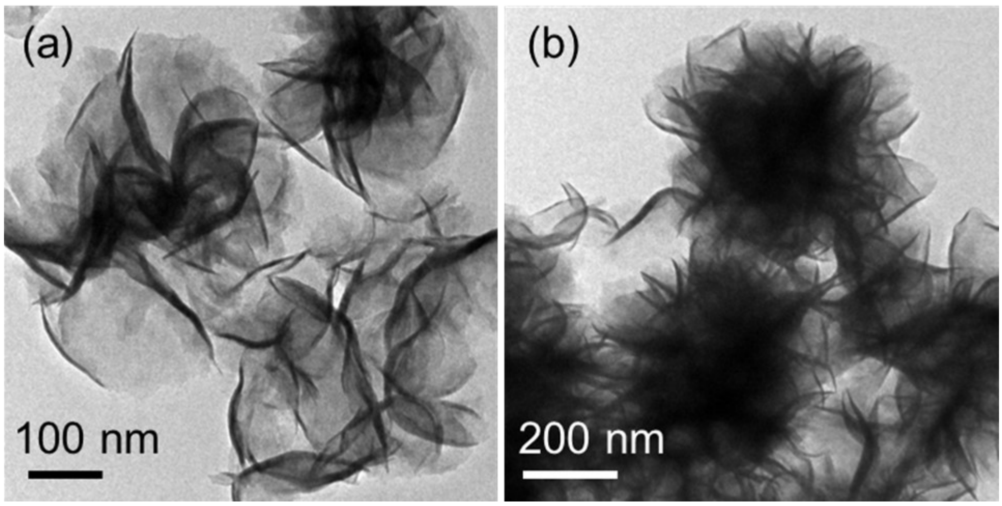

Figure S12. BF-TEM micrograph showing variation in size of MoS_2 obtained using **(a)** hydrated $W_{0.5}Mo_{0.5}O_3$, and **(b)** non-hydrated $W_{0.5}Mo_{0.5}O_3$.

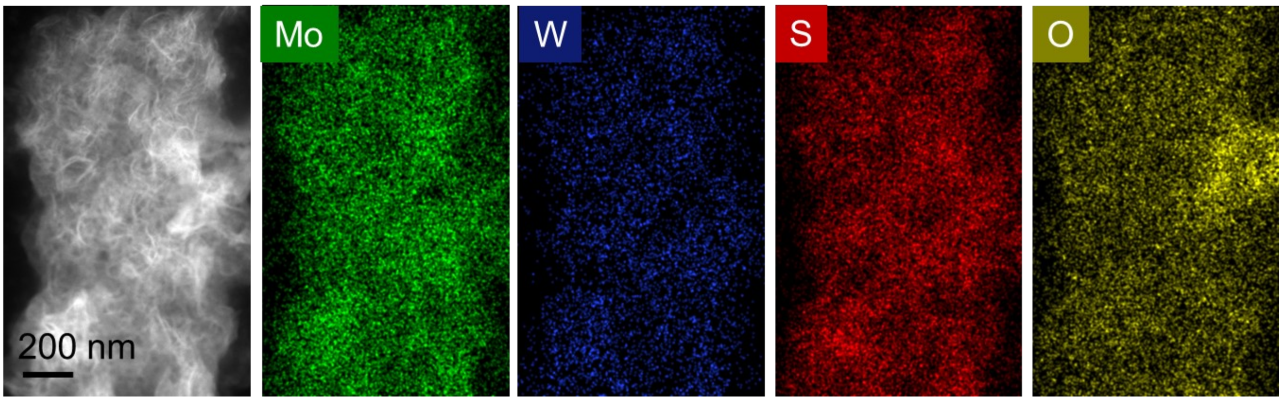

Figure S13. Time dependent experiment; HAADF-STEM micrograph of 6 h sulfurized product using non-hydrated $W_{0.5}Mo_{0.5}O_3$ and corresponding EDS maps showing elemental distribution of Mo, W, S, and O, respectively.

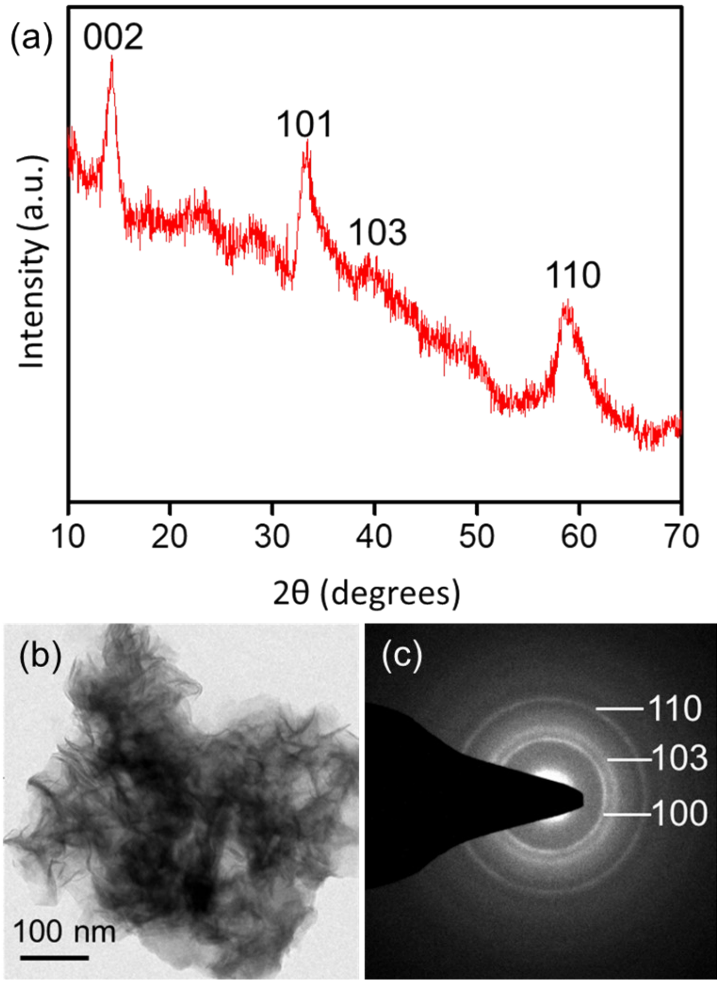

Figure S14. (a) Powder XRD pattern of pristine MoS_2 (synthesized separately using one-pot hydrothermal method); **(b)** BF-TEM micrograph, and **(c)** Diffraction pattern.

Characterization of pristine MoS_2

To correlate the physical and electrochemical properties of the MoS_2 synthesized using selective sulfurization of $W_{0.5}Mo_{0.5}O_3$ with that of MoS_2 reported in literature, pristine MoS_2 was prepared using a one-pot hydrothermal method. The characterization of this pristine MoS_2 is shown in **Figure S14**. **Figure S14(a)** depicts the powder XRD pattern of as-synthesized MoS_2, completely matches with JCPDS card no. 06-0097 with lattice parameters a = b = 3.16 Å, c = 12.295 Å, suggesting phase pure synthesis. In **Figure S14(b-c)**, TEM micrograph and corresponding diffraction pattern is shown. Flower morphology with SAED containing rings pattern, depicts their polycrystalline behavior. The BET surface area and electrochemical properties of these MoS_2 flowers have been compared with MoS_2 prepared by sulfurization of $W_{0.5}Mo_{0.5}O_3$ to elucidate the influence of selective sulfurization process on the materials characteristics.

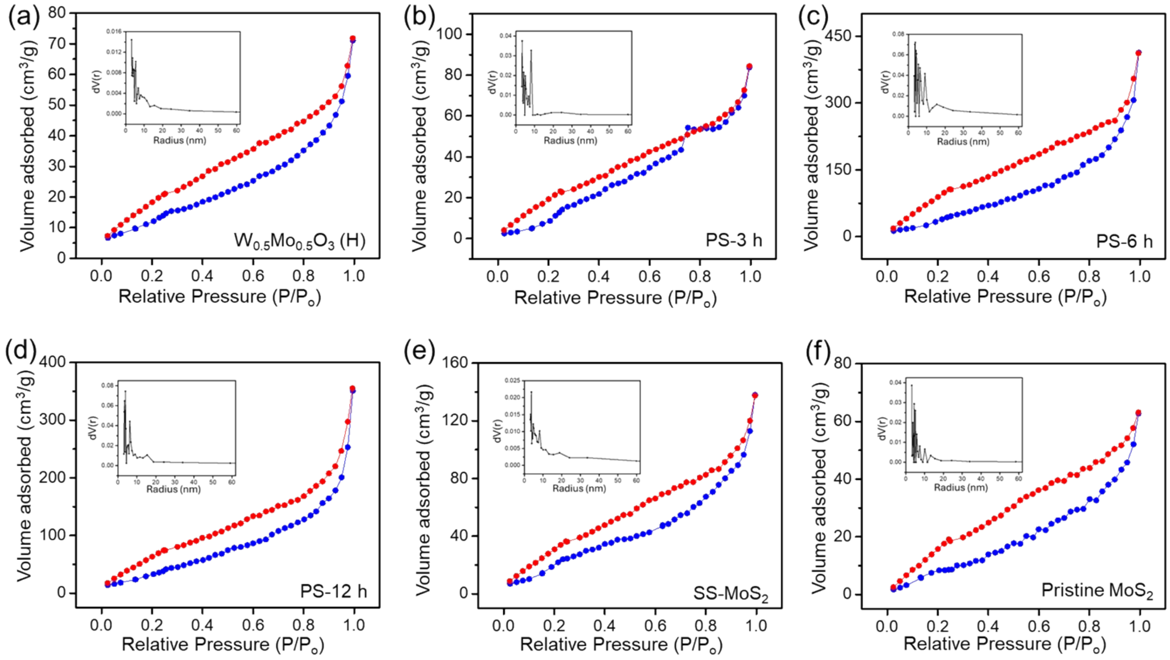

Figure S15. Nitrogen adsorption-desorption isotherms (BET plots) of **(a)** $W_{0.5}Mo_{0.5}O_3$ (H); **(b)** PS-3 h; **(c)** PS-6 h; **(d)** PS-12 h, **(e)** SS-MoS_2; and **(f)** Pristine MoS_2 (inset: Pore size distribution curves).

Table S3. Specific surface area, average pore size and average pore volume values of samples, obtained by BET and BJH method, respectively.

Sample	Surface area (m^2/g)	Average Pore size (nm)	Average Pore volume (cm^3/g)
$W_{0.5}Mo_{0.5}O_3$ (H)	53.9	3.15	0.10
PS-3 h	137.2	3.32	0.14
PS-6 h	229.6	3.72	0.65
PS-12 h	172.2	3.94	0.54
SS-MoS_2	122.1	3.73	0.30
Pristine MoS_2	45.4	3.14	0.11

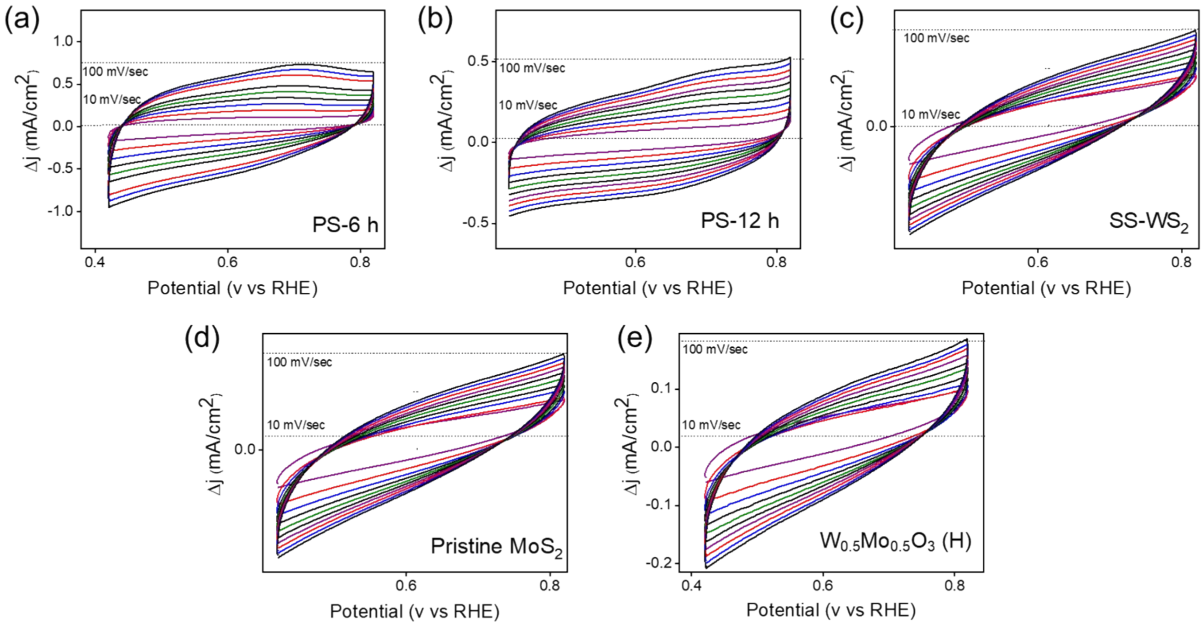

Figure S16. Cyclic voltametric response of samples in the non-faradaic region near to the HER polarisation region in 0.5 M H_2SO_4 of **(a)** PS-6 h; **(b)** PS-12 h; **(c)** SS-MoS_2; **(d)** Pristine MoS_2 and **(e)** $W_{0.5}Mo_{0.5}O_3$ (H), respectively.

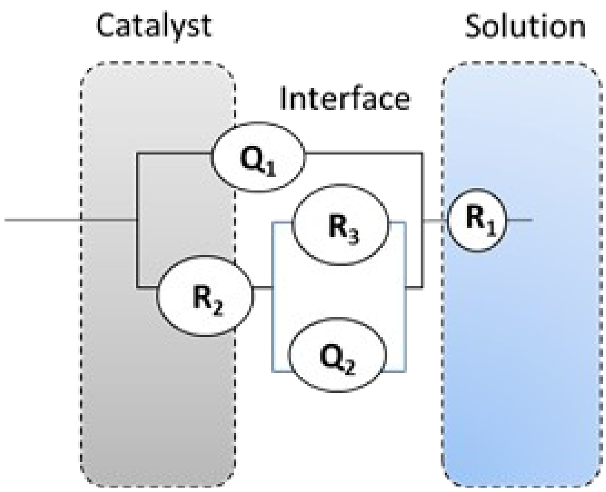

Figure S17: Equivalent circuit diagram used in EIS simulation.

Table S4: EIS circuit fitting for HER in 0.5 M H_2SO_4

Sample	R1(solution resistance)	R2 (Charge transfer resistance)	R3 (adsorption resistance)
PS-6 h	4.6	96.7	989
PS-12 h	2.9	51.6	738
SS-MoS_2	10.3	206.1	1224
$W_{0.5}Mo_{0.5}O_3$ (H)	1.2	541	2725
Pristine MoS_2	5.8	271	3538

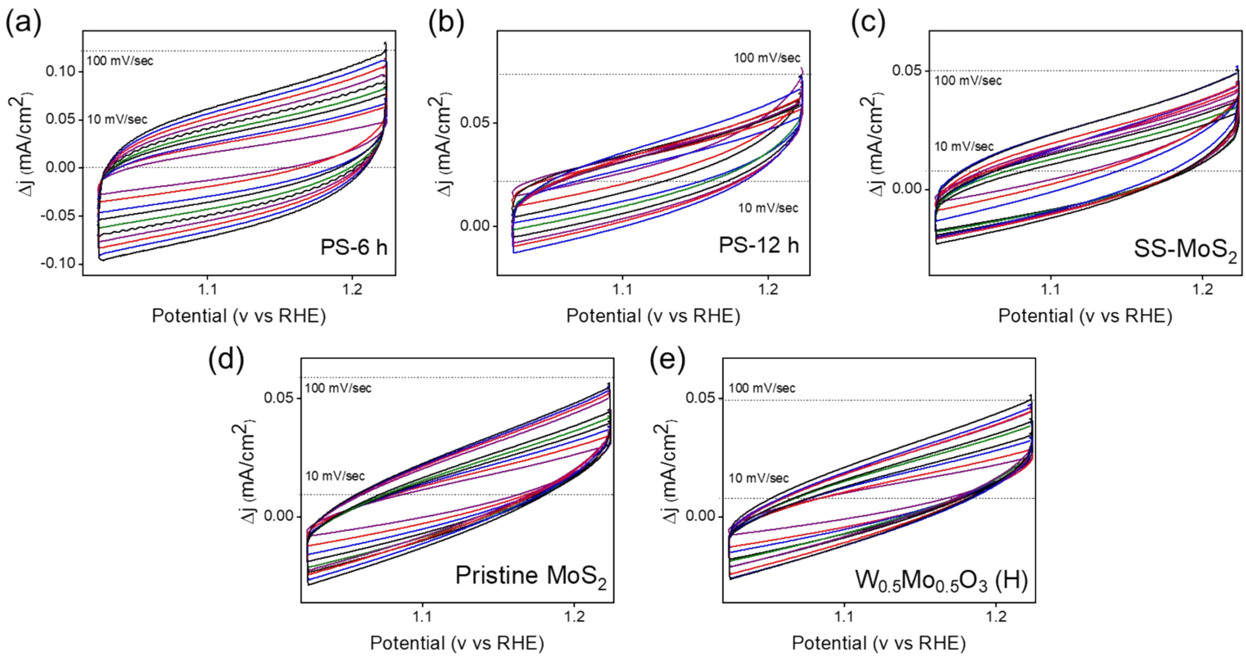

Figure S18. Cyclic voltametric response of samples in the non-faradaic region near to the OER polarisation region in 1M KOH of **(a)** PS-6 h; **(b)** PS-12 h; **(c)** SS-MoS_2; **(d)** Pristine MoS_2 and **(e)** $W_{0.5}Mo_{0.5}O_3$ (H), respectively.

Table S5: EIS circuit fitting for OER in 1 M KOH

Sample	R1(solution resistance)	R2 (Charge transfer resistance)	R3 (adsorption resistance)
PS-6 h	5.5	14.2	2.9
PS-12 h	5.6	11.8	9.4
SS-MoS_2	6.3	17.1	18.4
$W_{0.5}Mo_{0.5}O_3$ (H)	5	26.1	1159
Pristine MoS_2	4.6	36.6	4154

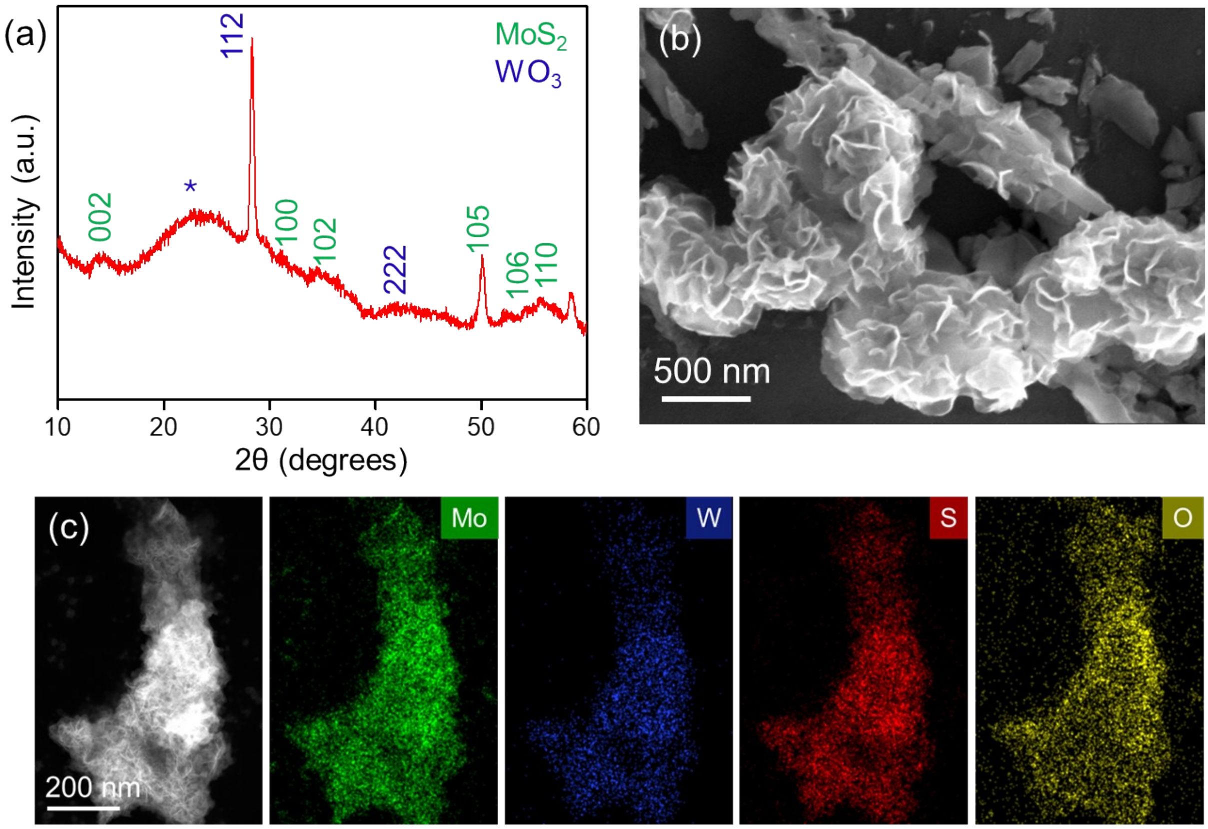

Figure S19. Post HER analysis of PS-6h sample; **(a)** PXRD pattern; **(b)** SEM micrograph; **(c)** HAADF-STEM micrograph and corresponding EDS maps of Mo, W, S and O elements in the sample.

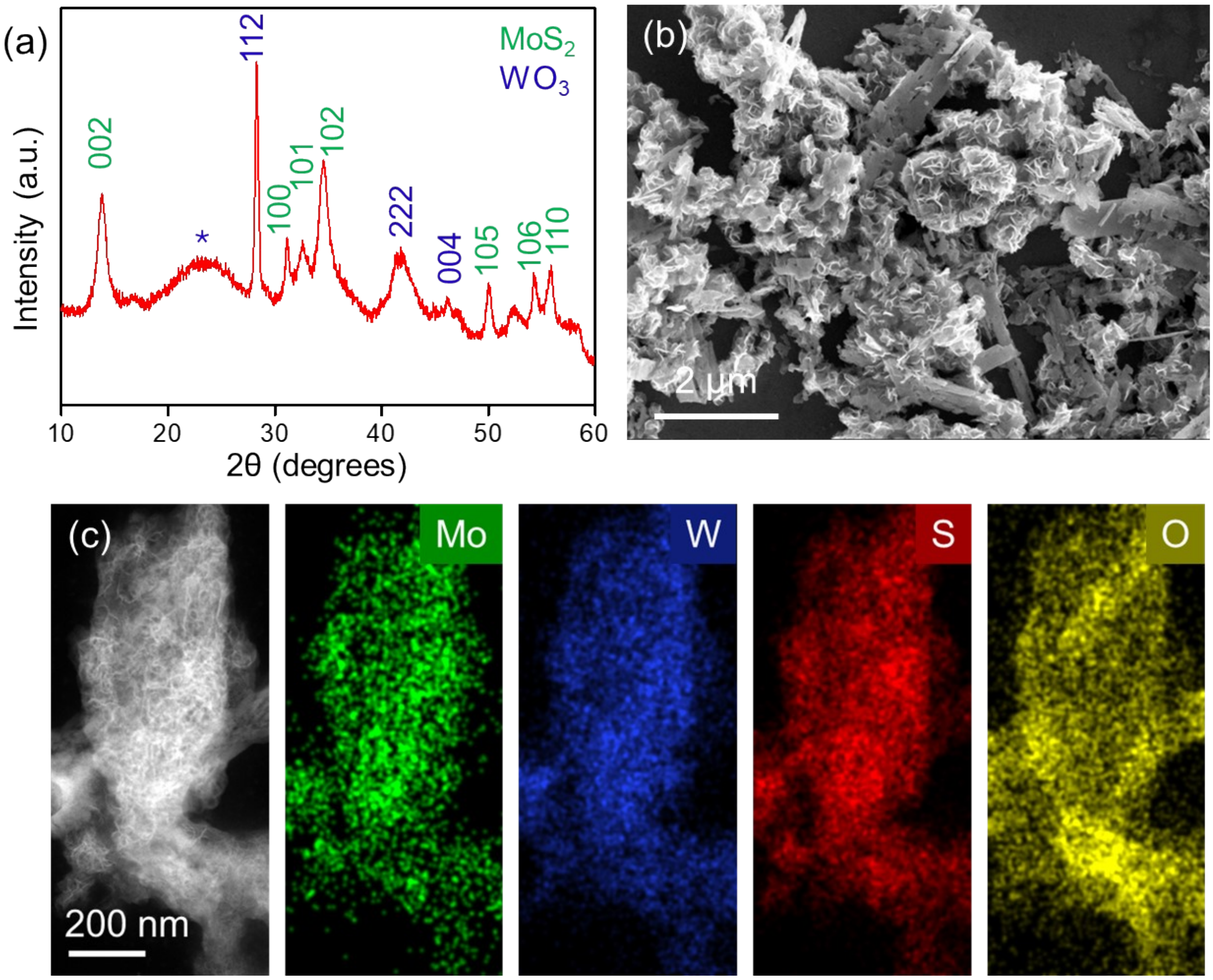

Figure S20. Post OER analysis of PS-6h sample; **(a)** PXRD pattern; **(b)** SEM micrograph; **(c)** HAADF-STEM micrograph and corresponding EDS maps of Mo, W, S and O elements in the sample.

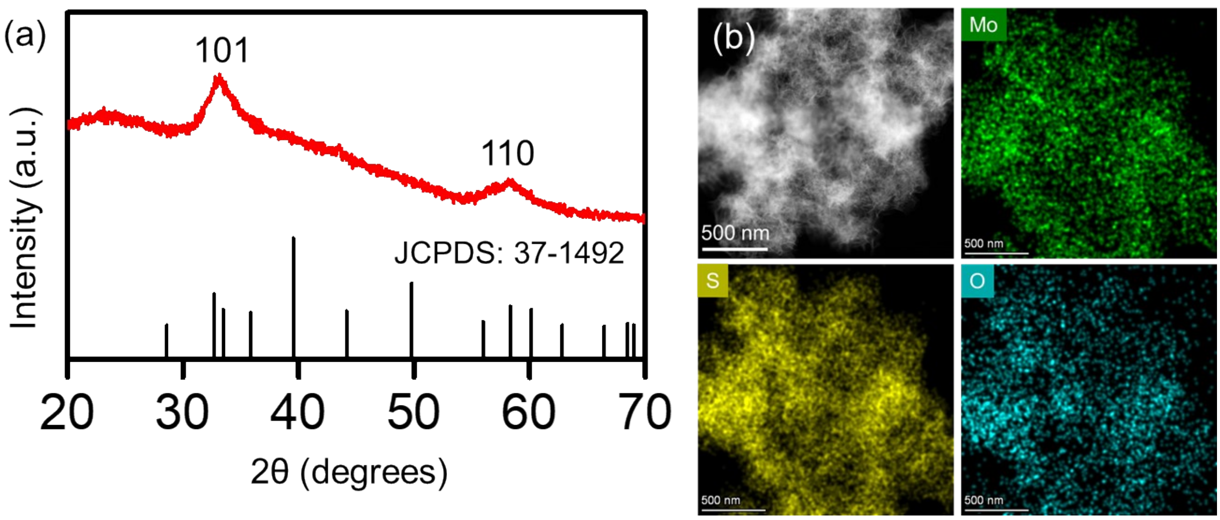

Figure S21. Post OER analysis of SS-MoS_2 sample; **(a)** PXRD pattern; **(b)** HAADF-STEM micrograph and corresponding EDS maps of Mo, S, and O elements in the sample.

Table S6. Comparison of HER and OER activity of previously reported MoS_2 and its heterostructures with our samples.

Sample	Reaction	Electrolyte media	Overpotential @ 10 mA/cm^2 (mV)	Tafel slope (mV/dec)	Stability 14h (% activity retention)	Reference
PS-6 h (MoS_2-WO_3 heterostructure)	HER	0.5 M H_2SO_4	211	123	95	This work
2H MoS_2	HER	0.5 M H_2SO_4	686	204	-	[1]
MoS_2 sheets	HER	0.5 M H_2SO_4	420	138	-	[2]
Etched MoS_2	HER	0.5 M H_2SO_4	267	136	-	[3]
SV-2H MoS_2	HER	0.5 M H_2SO_4	369	69	-	[1]
MoS_2/Nb_2CT_x	HER	0.5 M H_2SO_4	138	94	~70	[4]
FeS_2-MoS_2	HER	0.5 M H_2SO_4	136	82	-	[5]
Ni-MoS_2	HER	0.5 M H_2SO_4	302	67	-	[6]

1T-2H MoS_2	HER	0.5 M H_2SO_4	212	78	-	[7]
Mo_2N/CNT	HER	0.5 M H_2SO_4	218	133	~80	[8]
MoO_3-MoS_2	HER	0.5 M H_2SO_4	200	74	-	[9]
Co-BDC/MoS_2	HER	0.5 M H_2SO_4	248	86	~85	[10]
MoS_2/Ni QDs	HER	0.5 M H_2SO_4	450	105	-	[11]
MoS_2/graphene	HER	0.5 M H_2SO_4	30	67	-	[12]
MoS_2 ultrathin nanosheets	HER	0.5 M H_2SO_4	300	55	-	[13]
H-MoS	HER	0.5 M H_2SO_4	167	70	-	[14]
SV-MoS_2	HER	0.5 M H_2SO_4	170	60	-	[15]
PS-6 h (MoS_2-WO_3 heterostructure)	OER	1 M KOH	485	179	87	This work
MoS_2/Co-N-CN_2	OER	1 M KOH	442	169	~72	[16]
Co_9S_8@MoS_2	OER	1 M KOH	430	61	-	[17]
$Sr_2Fe_2O_6$@d	OER	0.1M KOH	600	60	-	[18]
Co-CoO/rGO	OER	1M KOH	390	68	97	[19]
MoS_2/BN	OER	1M KOH	770	190	-	[20]
BP/NS	OER	1M KOH	592	308	-	[21]
BP(Ni_2Fe_2)	OER	1M KOH	510	252	-	[22]
MoS_2/rGO-3%	OER	1M KOH	250	195	-	[23]
MoO_3	OER	1M KOH	644	89	-	[24]
Porous MoO_3	OER	1M KOH	510	125	83	[25]
MoS_2/NiS_2	OER	1M KOH	235	71	-	[26]
Ni-Mo-S@CC	OER	1M KOH	320	88	-	[27]
Co-Ru 1T MoS_2	OER	1M KOH	308	55	-	[28]
Fe/MoS_2/$CoMo_2S_4$	OER	1M KOH	290	65	-	[29]
M_1S_1	OER	1M KOH	300	220	-	[30]

Mo NC@MoS_2	OER	1M KOH	390	72	-	[31]
MoS_2/COF-C_4N	OER	1M KOH	349	64	79	[32]

References

1 C. Gu, T. Sun, Z. Wang, S. Jiang and Z. Wang, *Small Methods*, 2023, **7**, 2201529.

2 X. Yin, Y. Li, H. Meng and W. Wu, *Appl. Surf. Sci.*, 2019, **486**, 362–370.

3 R. Zhang, M. Zhang, H. Yang, G. Li, S. Xing, M. Li, Y. Xu, Q. Zhang, S. Hu, H. Liao and Y. Cao, *Small Methods*, 2021, **5**, 2100612.

4 L. Hu, Y. Sun, S.-J. Gong, H. Zong, K. Yu and Z. Zhu, *New J. Chem.*, 2020, **44**, 7902–7911.

5 X. Zhao, X. Ma, Q. Lu, Q. Li, C. Han, Z. Xing and X. Yang, *Electrochim. Acta*, 2017, **249**, 72–78.

6 P. Sundara Venkatesh, N. Kannan, M. Ganesh Babu, G. Paulraj and K. Jeganathan, *Int. J. Hydrogen Energy*, 2022, **47**, 37256–37263.

7 Z. Hong, W. Hong, B. Wang, Q. Cai, X. He and W. Liu, *Chem. Eng. J.*, 2023, **460**, 141858.

8 M. Meng, H. Yan, Y. Jiao, A. Wu, X. Zhang, R. Wang and C. Tian, *RSC Adv.*, 2016, **6**, 29303–29307.

9 X. Hou, A. Mensah, M. Zhao, Y. Cai and Q. Wei, *Appl. Surf. Sci.*, 2020, **529**, 147115.

10 D. Zhu, J. Liu, Y. Zhao, Y. Zheng and S.-Z. Qiao, *Small*, 2019, **15**, 1805511.

11 B. Lai, S. C. Singh, J. K. Bindra, C. S. Saraj, A. Shukla, T. P. Yadav, W. Wu, S. A. McGill, N. S. Dalal, A. Srivastava and C. Guo, *Mater. Today Chem.*, 2019, **14**, 100207.

12 L. Ma, Y. Hu, G. Zhu, R. Chen, T. Chen, H. Lu, Y. Wang, J. Liang, H. Liu, C. Yan, Z. Tie, Z. Jin and J. Liu, *Chem. Mater.*, 2016, **28**, 5733–5742.

13 J. Xie, J. Zhang, S. Li, F. Grote, X. Zhang, H. Zhang, R. Wang, Y. Lei, B. Pan and Y. Xie, *J. Am. Chem. Soc.*, 2013, **135**, 17881–17888.

14 J. Zhang, S. Liu, H. Liang, R. Dong and X. Feng, *Adv. Mater.*, 2015, **27**, 7426–7431.

15 H. Li, C. Tsai, A. L. Koh, L. Cai, A. W. Contryman, A. H. Fragapane, J. Zhao, H. S. Han, H. C. Manoharan, F. Abild-Pedersen, J. K. Nørskov and X. Zheng, *Nat. Mater.*, 2016, **15**, 48–53.

16 X. Hou, H. Zhou, M. Zhao, Y. Cai and Q. Wei, *ACS Sustain. Chem. Eng.*, 2020, **8**, 5724–5733.

17 H. Zhu, J. Zhang, R. Yanzhang, M. Du, Q. Wang, G. Gao, J. Wu, G. Wu, M. Zhang, B. Liu, J. Yao and X. Zhang, *Adv. Mater.*, 2015, **27**, 4752–4759.

18 R. K. Hona and F. Ramezanipour, *Angew. Chemie Int. Ed.*, 2019, **58**, 2060–2063.

19 X. Liu, W. Liu, M. Ko, M. Park, M. G. Kim, P. Oh, S. Chae, S. Park, A. Casimir, G. Wu and J. Cho, *Adv. Funct. Mater.*, 2015, **25**, 5799–5808.

20 J. Hou, Y. Sun, Y. Wu, S. Cao and L. Sun, *Adv. Funct. Mater.*, 2018, **28**, 1704447.

21 Q. Xu, J. Zhang, H. Zhang, L. Zhang, L. Chen, Y. Hu, H. Jiang and C. Li, *Energy Environ. Sci.*, 2021, **14**, 5228–5259.

22 X. Deng, R. Zhang, Q. Li, W. Gu and L. Hao, *ChemistrySelect*, 2022, **7**, e202200091.

23 M. S. Khan, T. Noor, E. Pervaiz, N. Iqbal and N. Zaman, *RSC Adv.*, 2024, **14**, 12742–12753.

24 S. D. Raut, N. M. Shinde, B. G. Ghule, S. Kim, J. J. Pak, Q. Xia and R. S. Mane, *Chem. Eng. J.*, 2022, **433**, 133627.

25 M. Zhang, R. Li, D. Hu, X. Huang, Y. Liu and K. Yan, *J. Electroanal. Chem.*, 2019, **836**, 102–106.

26 J. Bao, Y. Zhou, Y. Zhang, X. Sheng, Y. Wang, S. Liang, C. Guo, W. Yang, T. Zhuang and Y. Hu, *J. Mater. Chem. A*, 2020, **8**, 22181–22190.

27 Y. Wang, W. Sun, X. Ling, X. Shi, L. Li, Y. Deng, C. An and X. Han, *Chem. – A Eur. J.*, 2020, **26**, 4097–4103.

28 I. S. Kwon, T. T. Debela, I. H. Kwak, Y. C. Park, J. Seo, J. Y. Shim, S. J. Yoo, J.-G. Kim, J. Park and H. S. Kang, *Small*, 2020, **16**, 2000081.

29 Y. Guo, J. Tang, J. Henzie, B. Jiang, W. Xia, T. Chen, Y. Bando, Y.-M. Kang, M. S. A. Hossain, Y. Sugahara and Y. Yamauchi, *ACS Nano*, 2020, **14**, 4141–4152.

30 B. Chen, P. Hu, F. Yang, X. Hua, F. F. Yang, F. Zhu, R. Sun, K. Hao, K. Wang and Z. Yin, *Small*, 2023, **19**, 2207177.

31 I. S. Amiinu, Z. Pu, X. Liu, K. A. Owusu, H. G. R. Monestel, F. O. Boakye, H. Zhang and S. Mu, *Adv. Funct. Mater.*, 2017, **27**, 1702300.

32 N. Zhang, Z. Yang, W. Liu, F. Zhang and H. Yan, *Catalysts*, , DOI:10.3390/catal13010090.